V.4 Study of Sand Production

V.4.1 Large-scale Apparatus for Evaluation of Sand Production

(1) Introduction

The first offshore production test was conducted in Daini Atsumi Knoll in the Eastern Nankai Trough in March 2013. During the six-day test, gas production using the depressurization method totaled approximately 120,000 m^3. Sand production was observed during the test and problems related to continuing stable gas production also emerged. In order to enable long-term stable gas production from the MH layer, we have developed large-scale apparatus for evaluating sand production, and conducted sand production tests using the artificial sand layer sample based on the field condition of the offshore production test.

(2) Apparatus for Sand Production Test

As shown in Fig. 1, the apparatus for the sand production test consists of a sand layer, a solid-liquid separation tank, and a pump. The size of the sand layer is about 1m in diameter and 60cm deep.

A total of 12 sensors are installed at the bottom of the soil layer to measure the pressure difference in the apparatus. A rubber balloon is placed in contact with the top of the soil layer when the lid is closed. There are two types of solid-liquid separation tanks: main and sub. A scale is installed at the lower part of the main separation tank near the soil layer side. It is possible to measure the amount of sand using this scale. Water is circulated in the apparatus by a water pump. An acrylic observation window is installed in order to observe the pipe of the apparatus.

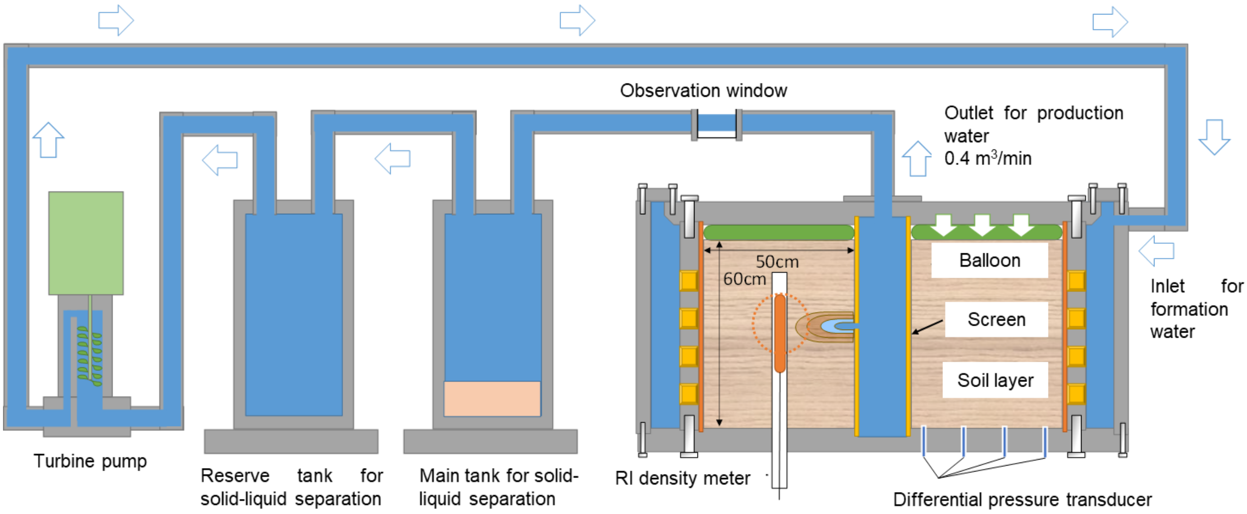

Fig.1 The Apparatus for sand production test

(Up) Photograph, (down) The schematic of the apparatus

The specifications of this apparatus are as follows:

- Volume of soil layer: 620 L
- Weight of soil layer: 1 ton
- Overburden pressure operated by balloon: Maximum 3 MPa, Back pressure: Maximum 1 MPa
- Pump: Maximum discharge: 0.4 m3/min (576 m3/day), Maximum head: 115.3 m (1.13 MPa)

(3) Example of circulation experiment

As shown in Fig. 2, we mixed No. 7 silica sand, No. 8 silica sand and fine sand and made the sand layer by referring to formation information of the offshore production test. A water pumping experiment was conducted in the sand layer for seven days. The results of this experiment are shown in Fig. 3. From the results of this experiment, it was confirmed that migration of fine sand is likely to occur. However, sand production was not observed. Although complex conditions in the field could not be sufficiently reproduced, it is considered possible to conduct laboratory experiments to study sand production.

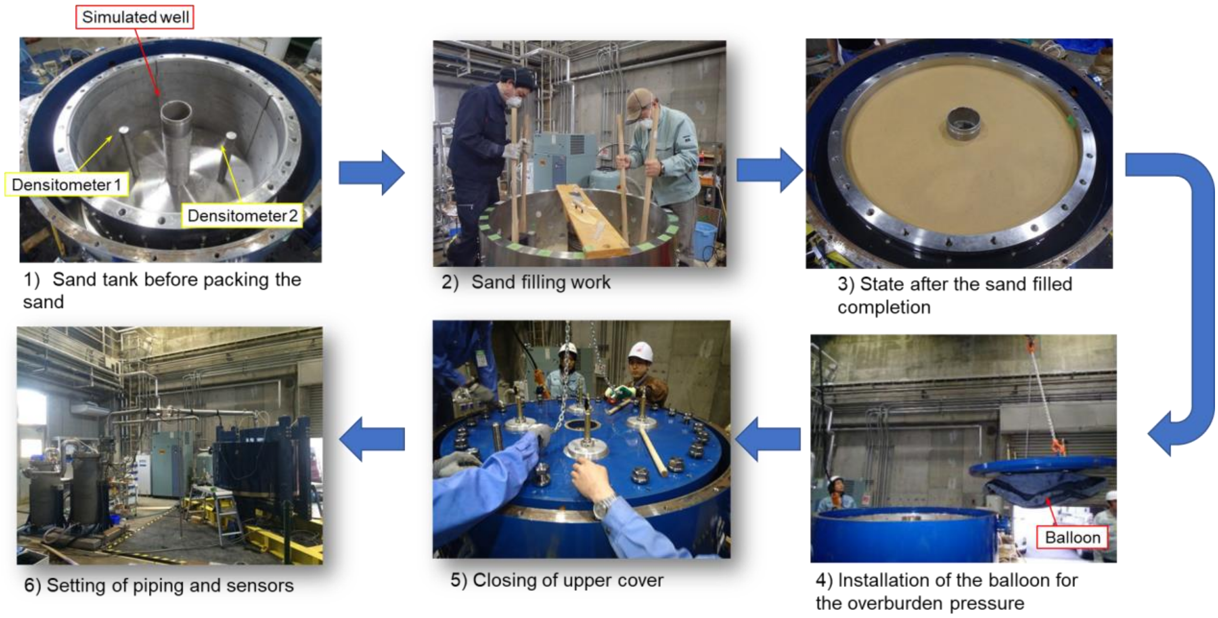

Fig.2 Step of preparation for experiment

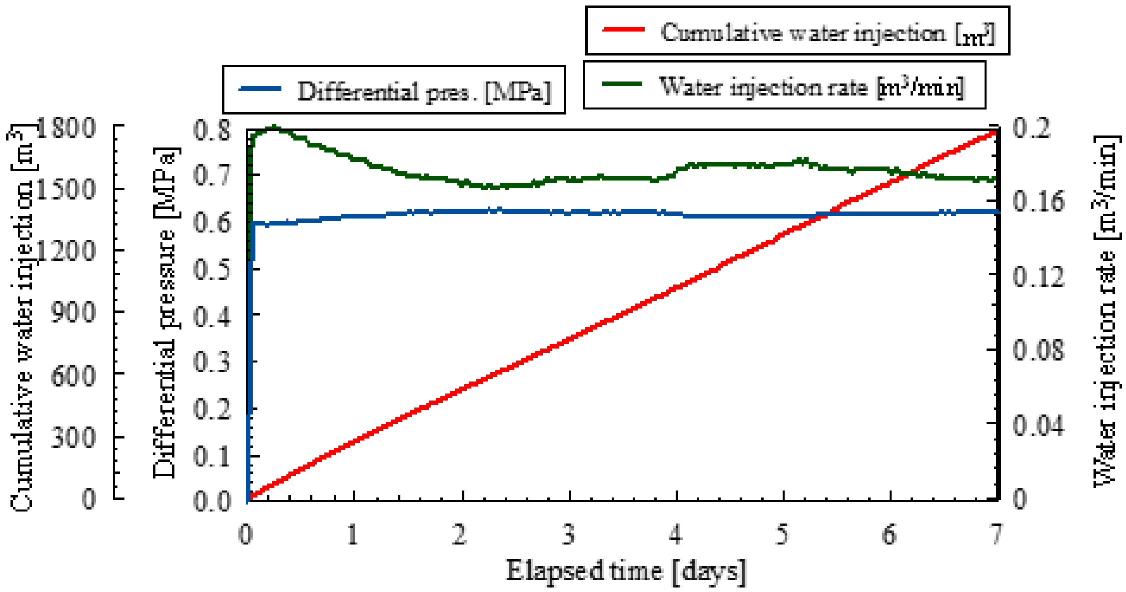

Fig. 3 Results of experiment

V.5 Study of Flow Assurance

V.5.1 Visualization Experiment

(1) Objective

The objective of this study is to understand the phenomena of hydrate regeneration during transportation of the produced gas from MH, and the possibility of plugging by such regenerated hydrate.

(2) Background

In the first offshore production test, a system was designed to separate gas and water inside the well and transport them separately to the onboard facility. In this system, there was a possibility that the temperature and pressure conditions inside the water production line around the seabed would get into the stability zone of the hydrate depending on operation conditions, which might cause plugging by the regenerated hydrate if gas flowed into the water production line. However, when this study was started, there were only a few cases where the effects of hydrate regeneration in the dynamic flow environment were studied, and there was no sufficient knowledge to study hydrate regeneration accompanying transport of production fluid. Therefore, with the aim of deepening this knowledge and reducing risks in terms of flow assurance in the offshore production test, we commissioned Oilfield Production Technology (currently Oilfield Technology) in 2011 and started carrying out examinations using visualization experiments.

Regarding the first offshore production test, possibilities of regeneration of hydrate and plugging by this hydrate under flowing conditions that included water and methane were considered. After the first offshore production test, the effects of high salinity were additionally considered, due to the high salinity of produced water confirmed in the test. Furthermore, prior to the second offshore production test, observation of bubble and hydrate particle sizes, accumulation and adhesion to the tube wall of hydrate, and properties of hydrate slurry on transportation were studied. From these results, models to consider hydrate regeneration under flow conditions and to estimate the apparent viscosity of hydrate slurry were examined.

(3) Details and Results

A) Consideration of Hydrate Regeneration and Plugging in the Flow

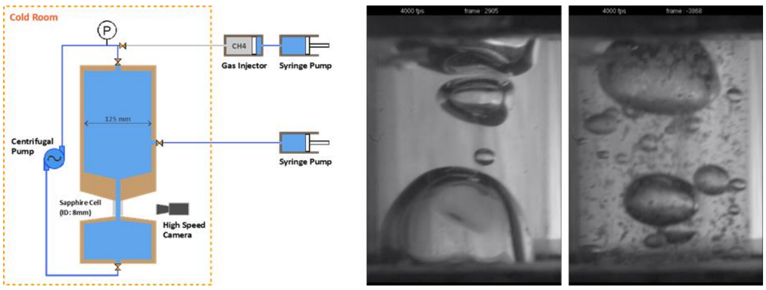

Fig.1 Outline of equipment used in initial experiment and visualized flow status

For the first step of the study, started in 2011, experiments to understand the process of hydrate regeneration in the flow were conducted. [1] Using a pressure vessel with an observation window made of sapphire glass, regeneration of hydrate in the flow condition with a qualitative change of viscosity was visually confirmed. A laser and high speed camera were used to visualize the change. (Fig.1)

The next step of the study was to confirm the possibility of plugging in the flow path of the system used in the first offshore production test. [2] In this experiment, a newly constructed flow loop was used. In the flow loop, transparent pipes were used for horizontal, vertical, corner, and dead end sections, which are the major components of the flow path, for visualization. By this visualization, observation of regeneration and accumulation of hydrate under flow became possible. In addition, to enable quantitative evaluation of apparent viscosity during the regeneration of hydrate, flow volume and density were measured. These results suggested that the possibility of plugging under flowing conditions is low, and the possibility of production failures caused by accumulation of hydrate in the BOP was also low. [3]

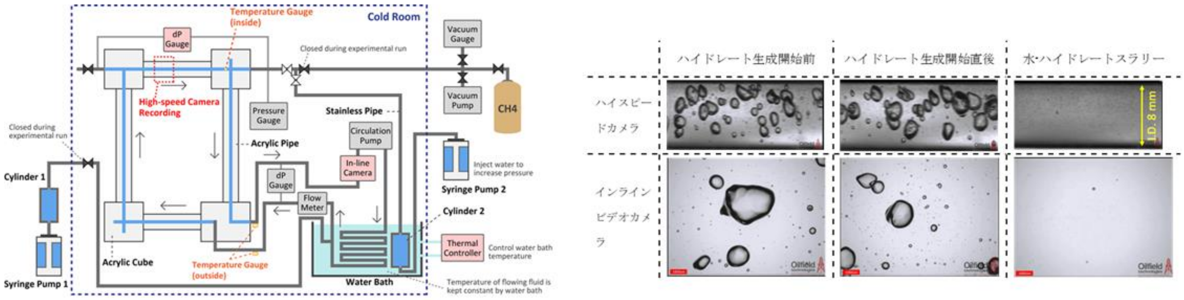

Fig.2 Outline of flow loop and visualized flow

For the experimental consideration after the first offshore production test, the effects of salinity were considered because the existence of high salinity was confirmed from the produced water. Also, the effects of fine particles were considered in relation to the sand production that occurred during the production test. [4] As a result, pressure to regenerate hydrate was affected by changes in salinity, however, no significant effects were confirmed in terms of the existence of fine particles.

From 2015, a study considering the second offshore production test was started. Through the detailed studies including experiments, we found there were some relations between problems of flow assurance (e.g. hydrate accumulation, adhesion to the tube wall) and flow velocity and/or shape of flow path. [2][3] On the other hand, the relationship between elements such as “volume ratio of methane gas and generated hydrate” and “bubble size of methane gas in flow and hydrate particle size” against the problems involving flow assurance had not been clarified. To solve these problems, models for estimating regeneration of hydrate and apparent viscosity were built based on the experiments using flow loop and detailed analysis of measured data. In addition, the application scope of the built model was considered.

B) Investigation of Bubble Flow Behavior for Gas-Water Separation

To investigate the gas-water separation, the size of the bubble of the gas that flows into the well is an important factor. Prior to the first offshore production test, an experimental study to identify bubble size after it passes through the gravel pack was conducted by Fukada Geological Institute. [1] Due to the limitation of the experimental system, gas was injected through the gravel under static conditions to confirm the size of the bubble that will be flowing into the system. From this experiment, the effect of gravel and flow volume was confirmed.

For the second offshore production test, the design of the downhole production system was revised to solve the gas-water separation issue confirmed in the first offshore production test. To understand the flow behavior of two-phase flow of gas and water, a visualization experiment to confirm the size of the bubble passing through the bead inserts was also conducted using the conditions of the second offshore production test.

C) Consideration of Gas-Water Separation in Second Offshore Production Test

In the first offshore production test, gas and water was to be separated downhole, however, it did not work as planned. The downhole production system was revised for the second offshore production test in order to attain more effective gas-water separation.

However, in one of the two wells, still gas-water separation was not sufficient and as a result, some gas was produced through the water production line.

In response to this, the possibility of gas bubbles flowing into the ESP was evaluated by carrying out numerical calculations of flow behavior around the ESP and the dual tubing section.

References

[1] Shunsuke Sakurai・Yoshihiro Terao・Yoshihiro Nakatsuka, 2012 : Flow Assurance Study for the Production System, 2011 JOGMEC Oil & Gas Technical Activity Report、187-190

[2] Shunsuke Sakurai・Yoshihiro Nakatsuka・Toshiyasu Ukita, 2013 : Flow Assurance Study for the Gas Production Test, 2012 JOGMEC Oil & Gas Technical Activity Report, 252-254

[3] Sakurai, S., Nakatsuka, Y., Edwards, T.J., Hoskin, B.J., Manning, D.K., 2014: An Experimental Study for Flow Assurance of the Methane Hydrate Production Test System. In: Offshore Technology Conference.

[4] Shunsuke Sakurai・Yoshihiro Nakatsuka, 2015 : Fluid Flow Behavior in a Water Production Line, JOGMEC Oil & Gas Technical Activity Report April2014 - March2015, 125-127

[5] Tomoya Nonoue・Shunsuke Sakurai, 、2016 : Fluid Behavior of the Water Dominant Gas-Water Two Phase Flow, JOGMEC Oil & Gas Technical Activity Report April2015 - March2016, 109-110

[6] Tomoya Nonoue, 、2017 : Fluid Behavior of Water-Dominant Gas–Water Two-Phase Flow, JOGMEC Oil & Gas Technical Activity Report April2016 - March2017, 153-155

[7] Tomoya Nonoue, 、2018 : Fluid Behavior of the Water-Dominant Gas-Water Two-Phase Flow, JOGMEC Oil & Gas Technical Activity Report April2017 - March2018, 1170-173

V.5.2 Experiment on Flow-Loop

(1) Introduction

In considering gas production from the MH layer, data of flow characteristics in saline-based multiphase flow under high pressure are important. From such a point of view, we acquired data of flow characteristics for saline-based multiphase flow under high pressure, and improved the technology contributing to the long-term stable production of gas. Specifically, we introduced flow-loop apparatus at a laboratory scale and a field scale experimental apparatus 28m high, and gained an understanding of the flow characteristics in the pipe.

(2) Overview of Flow-Loop Apparatus

A picture of the flow-loop apparatus is shown in Fig. 1. As shown in Fig. 2, the vertical up-flow section has pipes that are 1.5m long and with an inner diameter width of 5cm, whereas the inner diameter of the horizontal and the downflow sections is 2.1cm. The total flow-path length is 10.4m, and the total volume is 6.24 L. Viewing glass windows 8-mm in diameter are placed at the up-flow, the horizontal-flow, and the downflow sections. The centrifugal turbine pump is an electric submersible pump (ESP) installed in the bottom horizontal pipeline.

In the experimental study, the jetting pump flow at higher pressures could enhance microbubble stability[1]. Also, the water power of this apparatus is significantly lower than single phase flow even under high pressure conditions using the two phase flow pump[2], and the bubble generation process is estimated using image analysis[3]. In addition, we have acquired various data of flow patterns.

Fig. 1 Flow-loop apparatus

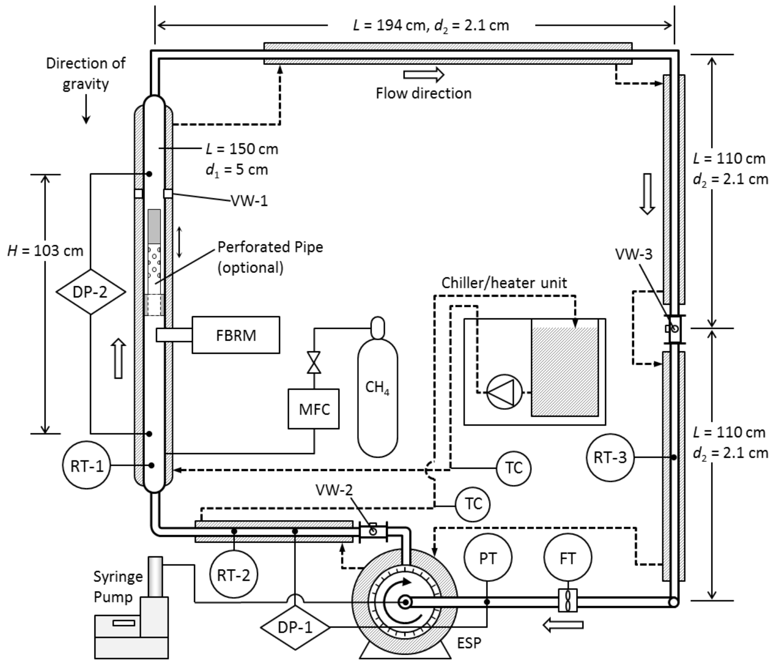

Fig.2 Schematic of flow-loop apparatus

PT: Pressure transducer, DP: Differential pressure transmitter,

RT: Resistance Thermometer, FT: Turbine flow meter, VW: viewing window

(3) Overview of Field Scale Experimental Apparatus

Fig. 3 shows the image and outline of the field scale experimental apparatus. The instrument consists of a 28m vertical pipe that simulates an offshore production well. This apparatus enables us to accumulate basic data of flow characteristics under operating conditions similar to those of offshore production, which are pressure and salinity ranges from 1.0 to 3.0 MPa and 0 to 7.0 wt%, superficial gas velocities of 0.25 to 2.0 m/s, and superficial liquid velocities of 0.25 to 1.2 m/s.

Regarding supplying gas and liquid from the bottom of the vertical pipe and splitting the mixture at the separator before gas is emitted from the top and liquid is discharged to the liquid separation line, we observed the effects of gas and liquid flow rates on flow patterns, as well as gas holdup under high pressure and salinity conditions. Fig. 4 shows an example of the experimental results. The results indicate that the gas holdup rises with the increase of superficial velocities of gas and liquid [4]. This is due to the increase of retention time and retained gas in the liquid phase caused by the generation of micro bubbles that is promoted by the increase in turbulence intensity of the flow field as superficial liquid velocity increases. By using this apparatus, we are able to obtain a range of information about the flow pattern.

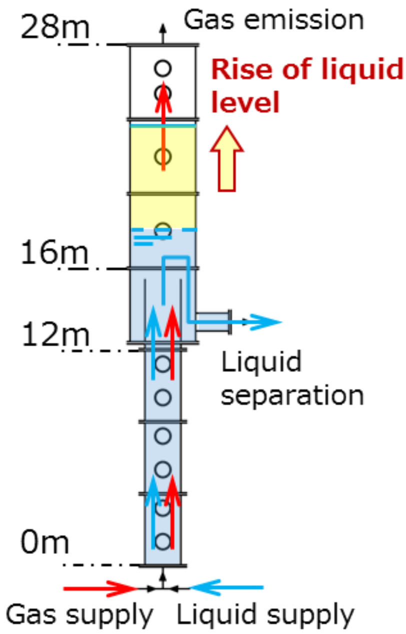

Fig.3 Image and outline of vertical pipe in field scale experimental apparatus

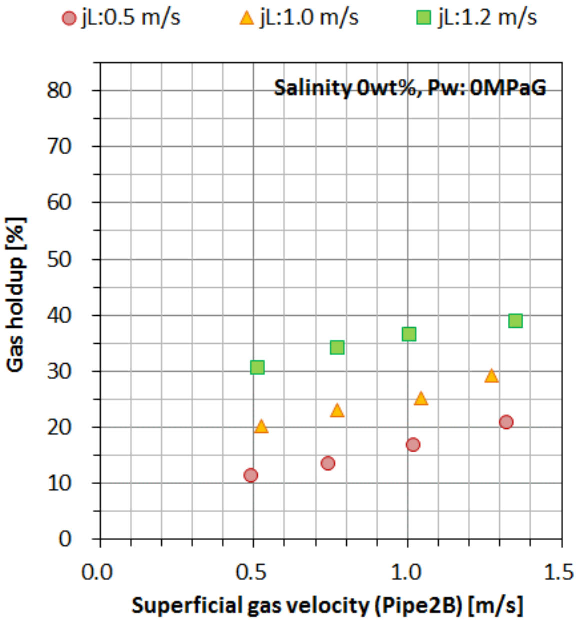

Fig. 4 Relationship between gas holdup and superficial gas velocity at various superficial liquid velocities.

(Superficial velocity based on 2 inch inner diameter, Pw: pressure (bottom of vertical pipe),

j_L: superficial liquid velocity)

References

[1] Shimizu, T., Yamamoto, Y., Tenma, N.、2016, : Shear-Induced Microbubble Generation at High Pressures， J. Chem. Eng. JPN, 49 (6), 519-525

[2] Shimizu, T., Yamamoto, T., Tenma, N., Narita, H.， 2015,: Electric Submersible Pump Performance under Methane/Water/Methane Hydrate Pipe Flows， Procs. 25th Int. Ocean and Polar Eng. Conf., ISOPE, 132-138

[3] Shimizu, T., Yamamoto, Y., Tenma, N.， 2016, Experimental Analysis of Two-Phase Flows and Turbine Pump Performance， Int. J. Offshore and Polar Eng., 26 (4), 371-377

[4] Shibata, N., Takahashi, M., Tenma, N., Moriya, H., Murayama, T., 2018. The study of the effect of pressure and sodium chloride concentration to Vertical upwards two-phase flow, Multiphase flow symposium.

V.6 Development of technology for advanced production method

V.6.1 Stimulation and Rehabilitation of Production Wells

(1) Introduction

To help ensure stable and long-term gas production, it is necessary to develop techniques that help prevent production damages associated with sand production, skin formations, lines clogging, soil consolidation, and re-formation of methane hydrates. For example, fine particles are likely to migrate near a wellbore and clog the pore spaces associated with gas production from methane hydrates in unconsolidated sand formations. If permeability decreases in the formation near the wellbore, gas production declines despite depressurization at the production well. As a countermeasure, we are studying an ultrasonic method to improve permeability. Because there is also concern about a reduction in permeability due to soil consolidation and reservoir compaction, feasibility of flow-path formation via hydraulic fracturing is also being examined.

(2) Ultrasonic Irradiation Method as a Countermeasure against Production Damage

Accompanied with advection of gas and water generated by depressurization of methane-hydrate reservoir, fine particles such as silt and clay contained in the reservoir may be transported toward the production well and accumulate nearby. If fine particles accumulate in the pore of skeleton particles, the permeability in the vicinity of the production well may decrease, which may lead to a reduction in the gas production rate. In addition, when a small-permeability layer, the so-called skin layer, is formed by the migration of fine particles, the pressure in the MH layer does not fall even if the pressure in the well is reduced, and the required amount of gas will not be able to be obtained.

Therefore, we are studying and developing a method to improve permeability of the near-well region by irradiating ultrasonic vibrations from the inside of the well. When a particle clogging a micro pore is subjected to ultrasonic vibrations, the particle is transported with the water and permeability improves.

Reservoir damage has been known to be related to the particle size and content of fine particles, the pore diameter of particles, and other factors. It is therefore necessary to continue examining the effects of improving permeability based on these factors in laboratory experiments. Specifically, using the sample of the particle-size distribution matched to the reservoir characteristics in the field, laboratory experiments have been carried out to gain an understanding of the effects of vibration, and to verify the effects of improving permeability using vibrations. Because the details of the clogging process cannot be confirmed in the actual production well, we are developing and testing a small-scale experimental device that can perform permeability experiments of one-dimensional flow, and a medium-sized experimental device that can handle radial flow.

As an example of a result, the improvement effect of the permeability by vibration using the small experimental device is shown in Fig. 2. In this experiment, when vibrations occur while the frequency is changed between several hundred Hz and 40 kHz, the most remarkable improvement was confirmed in the case of several tens kHz to 20 kHz. In addition, the sample was collected after the experiment and the distribution of the content of fine particles in the sample was examined. It has been confirmed that the amount of fine particles that can be removed (the influence range of vibrations) is the largest when vibration in the order of dozens of kHz to 20 kHz is applied.

In order to remove fine particles from the pores and improve the permeability in the one-dimensional flow experiment, a vibration frequency in the order of dozens of kHz to 20 kHz produced the most effective result. We are proceeding to acquire data on that vibration frequency when the scale is increased and with radial flow. We believe that conceptual design of equipment that can be applied in the field will be possible by making prototypes of vibrators necessary for indoor experiments, and accumulating data.

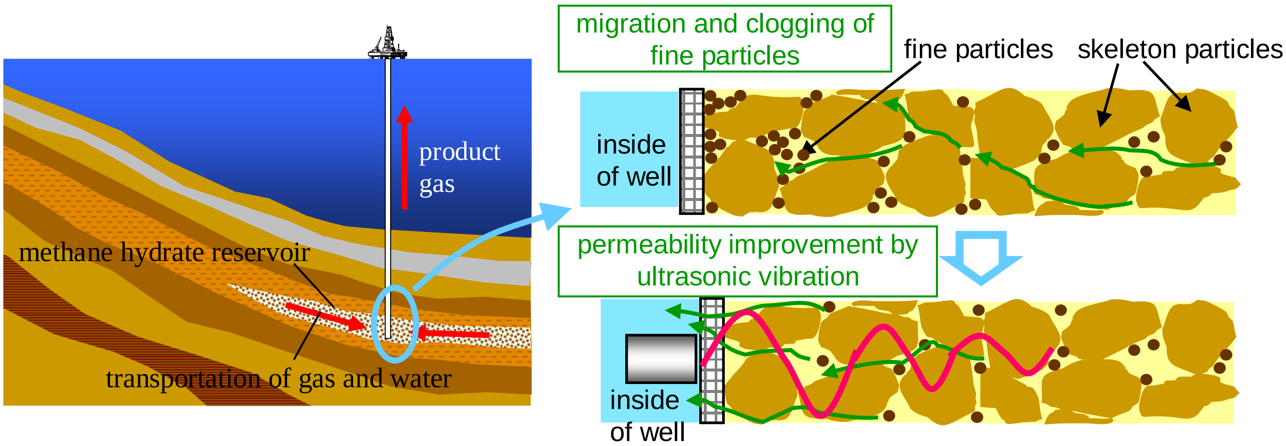

Fig.1 Application image of fine particle removal technology by ultrasonic vibration

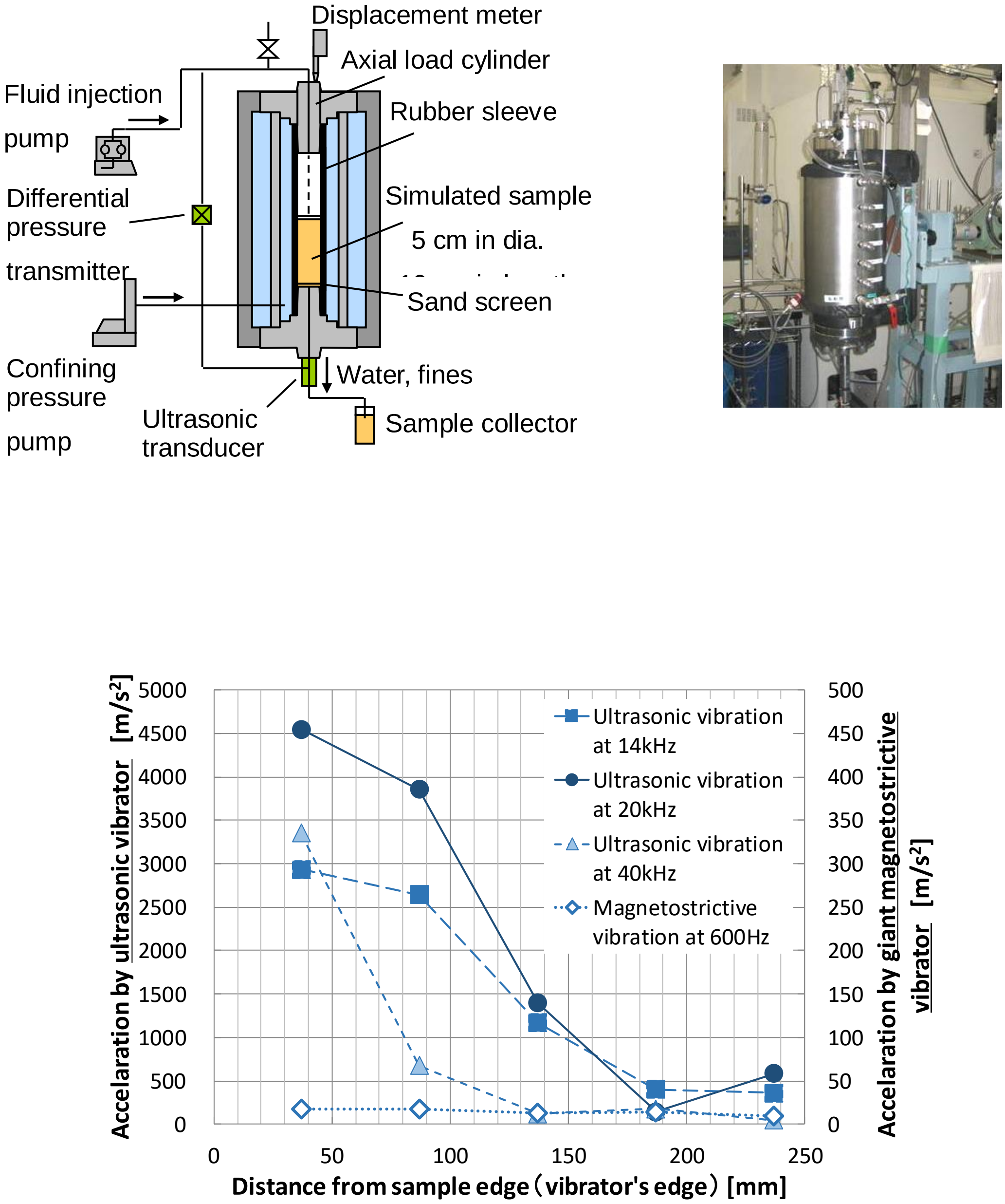

Fig. 2 Experimental apparatus and results with one dimensional flow
(Sample size: φ5cm x 10cm, small 1D equipment)

(3) Fracturing (Hydraulic Fracturing)

Depressurization will cause a substantial flow of water and gas from the reservoir to the wellbore, and in consideration of soft reservoir formation, i.e. unconsolidated sand, the fluid flow will force fine solids in the reservoir to move and accumulate around the wellbore. Furthermore, the drawdown will lead to formation compaction. Those events will result in undesirable and severe reduction in permeability in the near-well region. This situation can be improved by hydraulic fracturing. The created fracture will bypass the permeability reduction zone and rebuild the hydraulic communication between the wellbore and the reservoir, and it will also contribute to suppressing sand production. However, the mechanism of hydraulic fracturing in sands is not yet fully understood. Thus, we carried out laboratory experiments and numerical simulations based on DEM for this study.

In the experiments using a specimen made from a mixture of silica sand and kaolin, a linearly extending fracture was formed similarly as in the case of hard rocks when the proportion of kaolin was large. However, when the proportion of kaolin was small, no fracture was formed at all. These phenomena can be interpreted if the fracture is formed by compressive deformation/failure, which is completely different from the conventional theory of hydraulic fracturing. We also clarified that fracture behavior changes with fracturing fluids that differ in terms of viscosity and rheology. Those results show there is large potential for hydraulic fracturing to be applied to methane hydrate development[3]-[5].

(4) Summary

We introduced methods such as ultrasonic vibration and hydraulic fracturing as countermeasure against the reduction in permeability caused by skin formation and reservoir compaction.

With regard to the ultrasonic vibration method, we are also carried out investigations using laboratory experiments with radial flow of a larger scale after examination of one-dimensional flow. We determined that it is also necessary to develop and verify devices to enable them to be used in the field.

Furthermore, in order to apply the hydraulic fracturing method in the field, it is necessary to acquire data under more experimental conditions, and advance understanding of the mechanism by using numerical simulations and clarifying the applicable conditions.

References

[1] Tsuyuki K., Fujita Y., Miura S., Tajima D., 2014, Study on the measure of production damage by fine particles— About clogging formation by fine particles and the discharge of fine particles by vibration (in Japanese) -, Proceedings of 6th Methane Hydrate General Symposium, pp.80-85.

[2] Tsuyuki K., Miura S., Ebi T., Kitamoto Y., 2018, Improvement of permeability by vibration for measures against methane hydrate production damages —Relationship between vibration frequency and permeability improvement effect—(in Japanese), Proceedings of 73rd Annual academic lecture of the Japan Society of Civil Engineers, Ⅲ-147.

[3] Shimizu, H., Shazree, M., Ito, T., Narita, H. 2014, Flow-coupled DEM modeling for hydraulic fracturing in unconsolidated sands, *Proc. the 14th International Conference of the International Association for Computer Methods and Advances in Geomechanics* (14th ICIACMAG), MS 10-07.

[4] YoshikawaY., Shimizu H., Ito T., Tenma N. and Nagao J. 2016, Investigation of the factors influencing hydraulic fracturing behavior in unconsolidated sand by distinct element modeling, Proceedings of CSMH-8, 21-25.

[5] Ito T., and Tenma N., 2018, A basic study of fracture mechanics due to hydraulic fracturing in unconsolidated sands, Journal of the Japanese Association for Petroleum Technology, 83(6), 491-498

V.6.2 Enhanced Gas Recovery Method

(1) troduction

The depressurization method has been proposed as the most effective method for extracting methane gas from MH in marine sediments. In the dissociation process of MH, an endothermic reaction occurs. As the dissociation proceeds by heat supply using heat of the formation, undissociated MH may remain depending on the thermal balance. Therefore, we are also promoting research into enhanced gas recovery methods to obtain higher productivity and recovery rates.

(2) Deep Depressurization Method

Depressurization is a gas recovery method that uses reservoir heat for hydrate dissociation. The heat is generated by the temperature gap between initial and newly developed equilibrium conditions related to the production pressure. Thus, the gas production rate will decline after this heat is consumed. Generally, the recovery factor of the depressurization method is limited due to lack of heat. In this context, the deep depressurization method is studied as an enhanced recovery method. The deep depressurization method reduces the reservoir pressure below the quadruple point of methane hydrate (the point that hydrate, water, gas, and ice coexist. 273 K, 2.56 MPa) to intentionally form ice and use the latent heat of ice formation for hydrate dissociation. Laboratory experiments and numerical simulations were conducted to validate the effectiveness of the deep depressurization method [1] .

Figure 1 shows plant-scale equipment referred to as a High-pressure Giant Unit for Methane Hydrate Analyses: HiGUMA installed at the AIST Hokkaido center. Figure 2 shows the correlation between the recovery factor and temperature gaps (the initial temperature minus the dissociation temperature) when applying the normal depressurization and deep depressurization methods in the HiGUMA. In the process of normal depressurization, the recovery factor increased linearly due to the increase in reservoir heat lowering the dissociation temperature. On the other hand, by applying deep depressurization, the recovery factor was significantly improved due to heat supply by ice formation even though the temperature gap was constant. The results indicate that deep depressurization is promising as an enhanced recovery method, however, further analysis is needed to investigate negative effects such as hydrate reformation.

Fig. 1 Main pressure vessel of high-pressure giant unit for methane hydrate analyses

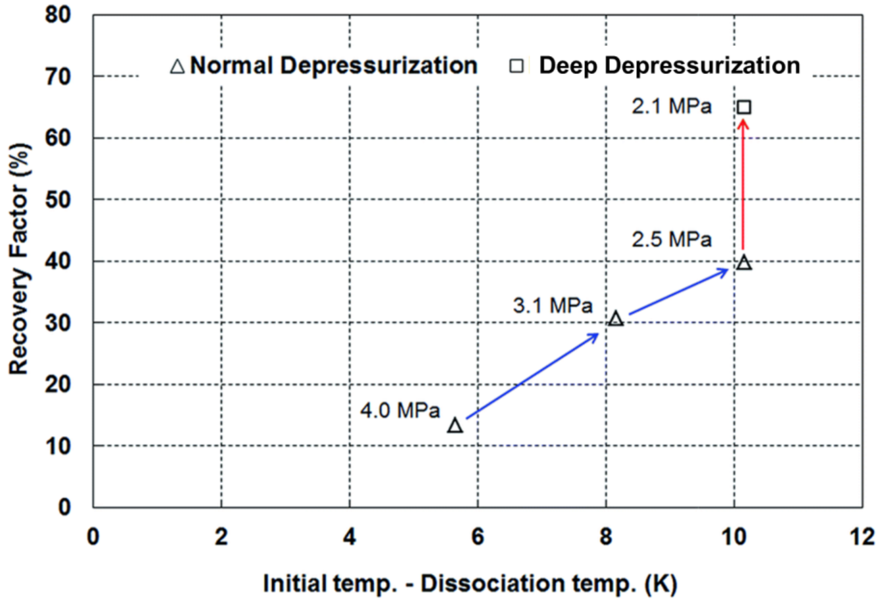

Fig. 2 Correlation between recovery factor and temperature gaps [2]

Reproduced from Ref. [2] with permission of the Royal Society of Chemistry

(3) Electrical Heating of Methane Hydrate Sediment for Gas Production

In-situ dissociation of natural gas hydrate is necessary in order to implement commercial recovery of natural gas from natural gas hydrate sediment. Thermal stimulation and depressurization are both effective dissociation methods. To simulate methane gas production from a methane hydrate (MH) layer, we used laboratory experiments to investigate the use of depressurization with additional electrical heating on MH sediment. Generally, electrical heating is used to produce crude oil and natural gas from wells. More specifically, the electric/electromagnetic enhanced oil recovery (EEOR) method has been applied to the recovery of heavy crude oil [3]. As shown in Figure 3, this is a very effective method for directly heating MH sediment with an electrical current, whereas hot water injection involves indirect heating using water. The EEOR method is advantageous due to its relative simplicity and because preferential heating with electrolyte solution causes less environmental pollution due to the use of an electrical network power supply. For crude oil production using the EEOR method, the main purpose of electrical heating is to reduce oil viscosity. For application to MH sediment, however, the EEOR method was developed to facilitate MH dissociation[4]. The efficiency of gas production due to electrical heating of a methane hydrate core was examined as a feasibility study of the methodology for safe commercial exploitation of methane hydrate as shown in Figure 4. In the case of low temperature conditions, which simulated a production well surrounding low thermal conductivity sediment, 37.2% of the hydrate remained in the sediment with depressurization alone, however, depressurization and additional electrical heating enhanced methane hydrate decomposition to >89% and produced the gas in a shorter period of time. With electrical heating, a reduction in core temperature due to the endothermic reaction of methane hydrate dissociation was suppressed and the core temperature increased by between 1°C and 4°C above the initial temperature. A current density of 10 A/m^2 for power of 1.6 W/kg with depressurization facilitated effective dissociation of hydrate. However, under high temperature conditions, which simulated a production well surrounding high thermal conductivity sediment, decomposition of methane hydrate was promoted by depressurization alone, and the increase in methane hydrate decomposition by additional electrical heating was less than 10%. Considering the application of electrical heating to an actual well, problems such as the electrical resistance and permeability are expected for practical use[5]. Furthermore, estimating the increase in MH dissociation volume that causes an increase in the electrical heating volume and a decrease in electric resistance is necessary. Therefore, combining depressurization and electrical heating of the hydrate layer is expected to be an effective method for enhancing gas production from the hydrate layer under low temperature or low thermal conductivity conditions.

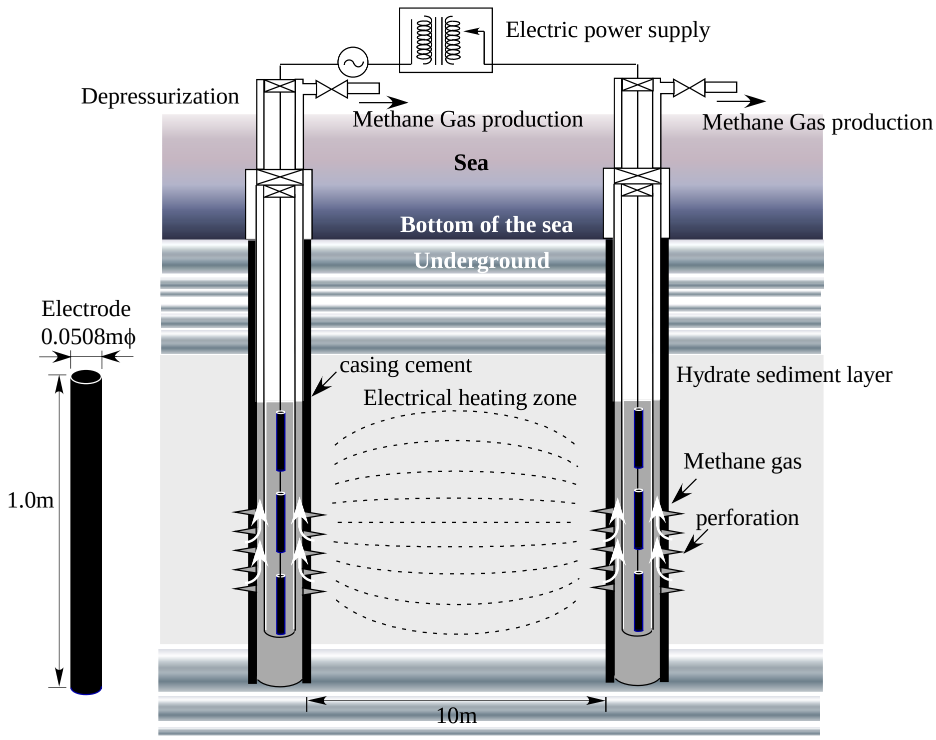

Fig. 3 Schematic of electrical heating by two electrode wells (5.04 cm in diameter × 1.0 m in length) separated by a distance of 10 m

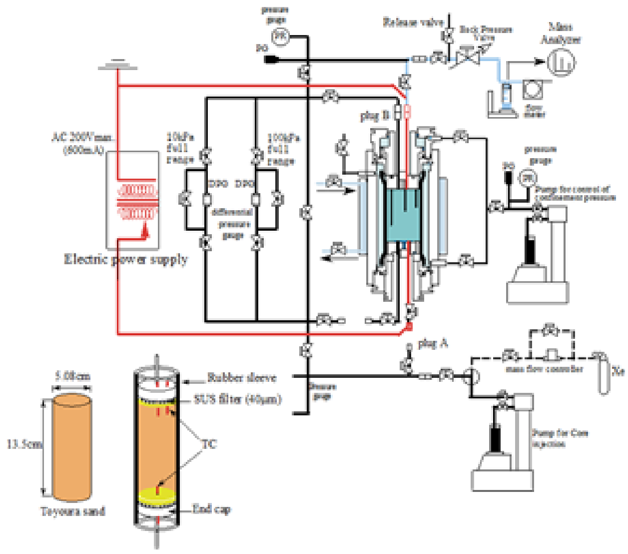

Fig. 4 Schematic diagram of apparatus for electrical heating and measuring water permeability

(4) CO_2-water Emulsion Injection Method.

The CO_2-water emulsion injection method is an option for enhanced recovery of methane hydrate by heating the production layers up to 10 degrees Celsius by a few degrees using exothermic heat of CO_2 hydrate. The quantity of exothermic heat that can warm the sand layers by 9 degrees Celsius is calculated by theoretical calculations and the numerical simulation using experimental results of injecting CO_2-water emulsion into saturated Toyoura sand of which porosity is 40% in a pressure cell [6] .

Then the field conditions for the CO_2-water emulsion method are considered step by step. As one example, almost the same amount of water and CO_2 are necessary to produce CO_2 hydrate in saturated layers. If the water from a production well could be used for the injecting emulsion, the applicability would be expanded. The formations of the emulsion using sea water and sodium chloride solutions are studied by using laboratory experiment in Figure 5. As another example, the liquid CO_2 droplets in the emulsion are refined into about 10 macro meters, the surface area in a unit volume is enlarged, and CO_2 hydrate formation is accelerated. Some confirmation experiments about the size of CO_2 droplets have also been carried out. In terms of field application of the method, the field injection device of CO_2-water emulsion has been conceptually designed as a first step, and the design parameters have been obtained.

Fig. 5 Laboratory experiments for CO_2-water emulsion injection method

(5) Partial Oxidation Method

The partial oxidation method is one of the enhanced production methods to obtain resources from MH layers. This method involves inputting a heat source by the oxidation of organic substances, and/or the combustion of a part of methane from MH that exists around the areas where heat is generated. In this study, we investigated the possibility of the utilization of partial oxidation method in order to dissociate MH as a heat source.

Figure 6 shows the schematic diagram of the partial oxidation method. It is assumed that the oxidation reaction proceeds in liquid-phase, because MH produces a large amount of water after dissociation and results in higher water saturation in the reservoirs. As a result, and through the experiments that simulate a low temperature and high pressure environment in porous media and/or around the injection wells [7], we confirmed that the increase in temperature occurs due to injection of acids into MH reservoirs. Furthermore, we accumulate fundamental data of various parameters, such as reaction rates and degree of heat generation caused by the oxidation of acid and solid materials, by using apparatus that simulates reservoir experimental apparatus. Based on the parameters obtained, a series of numerical simulations were carried out in order to ensure the possibility of the partial oxidation method as an EOR (Enhanced oil/gas recovery). The model used for the simulation has a porosity of 40%, and MH saturation 40%. As a result of simulating the acid injection process, it was discovered that the front of higher temperature with the formation of dissolution of mineral products expanded toward the direction of production wells, and that the higher production rate was obtained to promote dissociation of MH. The experiments also confirmed that the permeabilities in the reservoirs recovered due to the dissolution of porous media by the injection of acid solutions.

Furthermore, we obtained many practical results about the enhanced effects of MH production via the oxidation method as a result of carrying out the experiments, however, we also need to obtain fundamental data under different conditions.

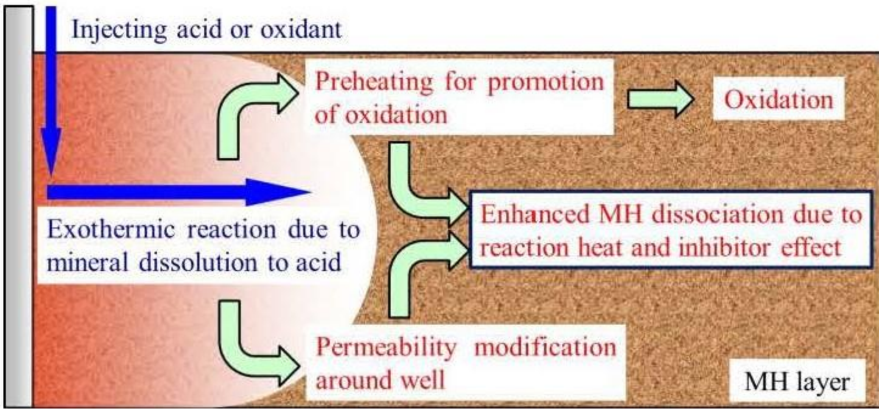

Fig. 6 Effects of enhanced production and recovery of permeability using partial oxidation method

References

[1] Konno, Y., Uchiumi, T., Oyama, H., Jin, Y., Nagao, J., Masuda, Y., and Ouchi, H., 2012: Dissociation Behavior of Methane Hydrate in Sandy Porous Media below the Quadruple Point, Energy Fuels, 26(7), 4310–4320

[2] Konno, Y., Jin, Y., Shinjou, K., Nagao, J., 2014: Experimental evaluation of the gas recovery factor of methane hydrate in sandy sediment, RSC Advances, 4, 51666

[3] Method of producing natural gas from a subterranean formation, United States Patent: 3916993, Katz; Marvin LaVerne (Dallas, TX)

[4] Minagawa, H., Ito, T., Kimura, S., Kaneko, H., Narita, h., 2014: Depressurization and Electrical Heating of Hydrate Sediment for Gas Production, INTERNATIONAL Journal of Offshore and Polar Engineering, Vol. 24, No.3, 218-223.

[5] Minagawa, H., Ito, T., Kimura, S., Kaneko, H., Noda, S., Tenma, N., 2017: Laboratory-scale Experiment of Depressurization and Electrical Heating of Methane Hydrate Sediment for Gas Production, Journal of Natural Gas Science and Engineering, Vol. 50, 147-156.

[6] Yojiro Ikegawa, 2007: Estimation by experiments and its analysis for thermal stimulation of methane

hydrate using exothermic reaction of CO2 hydrate formation, J. Japan Society of Civil Eng. -G, Vol.63, No.4.

[7] Nakano, Y., Kaneko, F., Sakamoto, Y. and Komai, T., 2018: Proceedings of the Twenty-eighth International Ocean and Polar Engineering Conference, 199-204

V.7. Metocean Study and Stability of Seabed

V.7.1 Metocean Study

V.7.1.1 Current Survey

(1) Objective and Background

The second offshore production test area is approximately 1,000m deep and corresponds to the north side of the Kuroshio Current axis, where the direct impact of the Kuroshio is small, however, this area is often affected by the meandering of the Kuroshio Current due to counter-current and divergent flow. In addition, as a result of short-term flow observations conducted in the past, it has been found that the surface, middle, and bottom flows are complicated in this area.

Consequently, it became necessary to study the riser behavior in such flow conditions.

Since the analysis of riser behavior requires long-term current flow data (direction and speed), one-year long-term current survey was conducted at three stations at the Daini-Atsumi Knoll.

(2) Details and Results

a. Details

The three red symbols [+] in Fig. 1 mark the locations of the deepwater current moorings [AC-1, AC-2, and AC-3].

Three deepwater mooring systems (Fig. 2) were deployed at the site to collect 12 months of data (from 7 December, 2011 to 11 December, 2012). Maintenance was conducted in March, June, and September 2012. During each maintenance period, the moorings were recovered and repaired; thereafter, data were downloaded and the moorings were redeployed. The design and deployment locations are provided in Tables 1 for the three moorings.

Table. 1: Summary of Design, and Deployment Position of Current Survey

Mooring No.	Observation Period(JST)		Location(WGS84)		Depth(m)
	Start	End	Latitude	Longitude	
AC-1	10-Dec-'11 12:00	08-Dec-'12 07:20	33° 56.683′ N	137° 17.992′ E	1135
AC-2	07-Dec-'11 15:20	11-Dec-'12 07:10	33° 53.883′ N	137° 15.757′ E	1278
AC-3	10-Dec-'11 15:50	07-Dec-'12 08:10	33° 55.862′ N	137° 19.923′ E	854

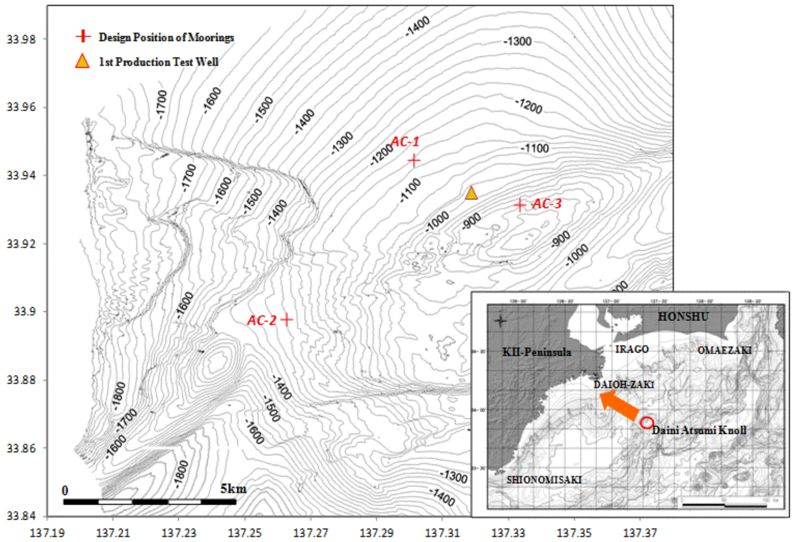

Fig.1: Location map of current survey

b. Results

1) Maximum Velocity and Average Velocity at Station AC-1

The maximum current speed during the observation period was 1.08m/sec at a depth of 75m, observed at 05:00 on October 8, 2012 (JST: Japan Standard Time), and the current direction at this time was 267°. The maximum current speed at other depths was 0.98m/sec (current direction 267°) at a depth of 171m [08:30 on July 25, 2012 (JST)], 0.79m/sec (current direction 337°) at a depth of 395m [16:40 on November 30, 2012 (JST)], 0.37m /sec (current direction 149°) at a depth of 859m [06:25 on November 10, 2012 (JST)], 0.51m/sec (current direction 52°) at a depth of 1,128m (7m ASB: Above Sea Bed) [12:00 on November 13, 2012 (JST)].

The mean current speed during the observation period was 0.37m/sec (75m deep), 0.33m/sec (171m deep), 0.22m/sec (392m deep), 0.09m/sec (859m deep), and 0.12m/sec (1,128m deep).

2) Maximum velocity and average velocity at station AC-2

The maximum current speed during the observation

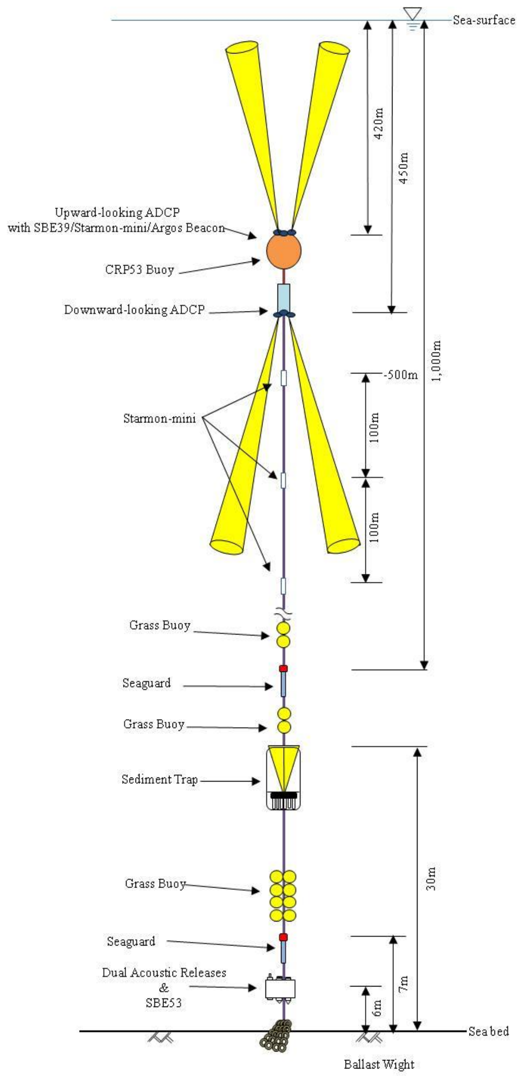

Fig.2: Mooring System

period was 1.22m/sec at a depth of 57m, observed at 23:20 on October 19, 2012 (JST), and the current direction at this time was 106°. The maximum speed at other depths was 1.05m/sec (current direction 205°) at a depth of 185m [06:10 on October 3, 2012 (JST)], 0.75m/sec (current direction 313°) at a depth of 393 m [06:20 on December 1, 2012 (JST)], 0.46m /sec (current direction 308°) at a depth of 839m [18:35 on June 20, 2012 (JST)], 0.58m/sec (current direction 328°) at a depth of 1,179m (7m ASB) [15:30 on August 3, 2012 (JST)].

The mean current speed during the observation period was 0.37m/sec (57m deep), 0.31m/sec (185m deep), 0.21m/sec (393m deep), 0.13m/sec (839m deep), and 0.10m/sec (1,179m deep).

3) Maximum Velocity and Average Velocity at Station AC-3

The maximum current speed during the observation period was 1.09m/sec at a depth of 49m, observed at 15:50 on January 21, 2012 (JST), and the current direction at this time was 247°. The maximum speed at other depths was 1.05m/sec (current direction 318°) at a depth of 177m [22:10 on November 25, 2012 (JST)], 0.73m/sec (current direction 326°) at a depth of 385 m [14:00 on November 30, 2012 (JST)], 0.51m /sec (current direction 259°) at a depth of 745m [06:55 on November 16, 2012 (JST)], 0.75m/sec (current direction 307°) at a depth of 847m (7m ASB) [15:30 on August 3, 2012 (JST)].

The mean current speed during the observation period was 0.38m/sec (49m deep), 0.33m/sec (177m deep), 0.23m/sec (385m deep), 0.14m/sec (745m deep), and 0.13m/sec (847m deep).

(3) Summary

a. Although the bottom flow of AC-3 on the northwest slope of the Daini-Atsumi Knoll shows a weak flow with a mean current speed (0.12m /sec), a strong northwest current of over 0.5m/sec is often measured in this area. Based on this observation, it is presumed that a strong bottom current appears around the ocean producing the test point near AC-3.

b. The characteristic of the current in this area is that the current directions of the upper layer, middle layer, lower layer, and bottom are completely different at a certain time.

c. The current in this area is influenced by tidal force, consequently the main direction is the northeast-southwest flow.

d. This area is strongly affected by warm water mass and cold water mass flowing in by counter-current and divergent flow due to the Kuroshio meander.

e. The bottom current on the northwest slope of the Daini-Atsumi Knoll is presumed to be affected by density current, bottom topography, and internal tides.

References

[1] E. Shimura and H. Okayama (2012): Current Measurment by Deepwater Mooring System, The 23rd Ocean Engineering Symposium, August 2-3, 2012.

[2] E. Shimura and H. Okayama (2013): Current Condition of the Daini-Atsumi Knoll, The 5th Comprehensive Symposium on Methane Hydrate (CSMH-5), AIST, pp.121-128.

V.7.1.2 Winds and Waves

(1) Objective and Background

Wind and wave conditions are the major external parameters that have a major impact on ships and floating structures, and in addition, these are essential elements when considering the limits of offshore operation. International standards such as the ISO (International Organization for Standardization) clearly define the expected values of the wind speed and wave height, which are limits when carrying out offshore operations. Therefore, in the case of offshore operations, it is necessary to calculate in advance the expected values associated with the return period in the production test site of the wind speed and wave height, etc., and to clearly define the work limit.

From the above, we calculated a maximum instantaneous wind speed (3-second mean wind speed), a 1-minute mean wind speed, a 10-minute mean wind speed, a 1-hour mean wind speed, the significant wave height and period, and the value associated with the return period (1 year, 5 years, 10 years, 25 years, 50 years, 100 years) and the Non-Exceedance Distributions (1- hour mean wind speed and significant wave height), etc. (Table.1)

Table. 1: Calculation Item

Item		Value associated with return period	Non-Exceedance Distributions	Note
Wind	U_{3sec} = 3-seconds extreme wind speed	○	−	$U_{3sec} = U_{max} = 1.25 \times U_{10min}$
	U_{1min} = 1-minute mean wind speed	○	−	$U_{1min} = 1.11 \times U_{10min}$
	U_{2min} = 2-minutes mean wind speed	○	−	$U_{2min} = 1.08 \times U_{10min}$
	U_{10min} = 10-minutes mean wind speed	○	−	Data Base (Japan Weather Association)
	U_{1hour} = 1-hour mean wind speed	○	○	$U_{1hour} = 0.92 \times U_{10min}$
Wave	$H_{1/3}$ = significant wave height	○	○	Data Base (Japan Weather Association)
	$T_{1/3}$ = significant wave period	○	−	$T_{1/3} = 4.1 \times \sqrt{H_{1/3}}$
	$L_{1/3}$ = wave length	○	−	$L_{1/3} = 1.56 \times {T_{1/3}}^2$
	H_{max} = maximum wave height	○	−	$H_{max} = 1.86 \times H_{1/3}$
	T_{max} = maximum wave period	○	−	$T_{max} \approx T_{1/3}$

(2) Details and Results

a. Details

For the analysis, data ("Global ocean hindcast database (1951-2013)" and "Ocean wave hindcast database around Japan (2001-2013)") for 63 years (1951-2013) estimated using the third generation wave spectrum model (WAM: Wave Modelling Group) based on the sea surface wind obtained by NECP model and GPV (JMA) model was used. (Table 2).

These data were corrected, assimilated, checked for accuracy, statistically processed to determine chronological change, and then “the appearance frequency”, “the value associated with return period”, and “the non-exceedance distributions” were calculated.

The return periods are 1, 5, 10, 25, 50, 100 years, and the non-exceedance distributions are 10, 20, 30, 40, 50, 60, 70, 80, 90, 91, 92, 93, 94, 95, 96, 97, 98, 99%.

Table. 2: Data Used For Analysis

Item	Detail
Area	Daini-Atsumi Knoll（33°56′ N、137°19′ E）
Data	**Japan Weather Association Wave prediction data base** ＜Global ocean hindcast database＞ outline：Wave prediction by ocean surface wind due to NCEP*1, JMA*2 GPV*3 Model Method：WAM (Wave Modering Group) period：1951～2013 resolution：0.5deg. ≒ 50km, time resolution 1hour item：mean wind speed & direction, significant wave height and period etc. ＜Ocean wave hindcast database around Japan＞ outline：Wave prediction by ocean surface wind due to JMA*2 GPV*3 Model Method：WAM (Wave Modering Group) period：2001～2013 resolution：2' (1/30deg. ≒ 3.7km、time resolution 1hour
Data period	1951～2013（60years）
Statistical processing (Frequency of appearance)	The wind speed, wave height, period, wave direction data were subjected to statistical processing to time series variation and appearance frequency and meteorological analysis.

Item	All year		Monthly	
	omniazimuth	the 16 points of the compass	omniazimuth	the 16 points of the compass
Frequency of appearance (Wave height)	○	○	○	○
Frequency of appearance (Wave period)	○	○	○	○
Frequency of appearance (height & period)	○	○	○	○
Frequency of appearance (Wind speed)	○	○	○	○

b. Results

1) Value Associated With Return Period

Table 3 shows the value associated with the return period (maximum instantaneous wind speed (3-second mean wind speed), 1- minute mean wind speed, a 10-minute mean wind speed, a 1-hour mean wind speed, the significant wave height and period).

Table.3: Value Associated with Return Period of Wind Speed and Waves

Return Period	Wind Speed				Waves			
	U_{3sec} (m/sec)	U_{1min} (m/sec)	U_{10min} (m/sec)	U_{1hour} (m/sec)	$H_{1/3}$ (m)	$T_{1/3}$ (sec)	$L_{1/3}$ (m)	H_{max} (m)
1yr	35.4	31.5	28.4	26.1	6.70	10.5	174	12.46
5yr	40.7	36.2	32.6	30.0	9.85	12.8	255	18.32
10yr	43.0	38.2	34.4	31.7	11.22	13.6	291	20.87
25yr	46.0	40.9	36.8	33.9	13.03	14.7	337	24.24
50yr	48.3	42.9	38.7	35.6	14.39	15.5	373	26.77
100yr	50.6	44.9	40.5	37.3	15.76	16.2	408	29.31

※$T_{max} \approx T_{1/3}$

2) Monthly and Annual Non-Exceedance Distributions

The non-exceedance distributions (1-hour mean wind speed and significant wave height) are shown in Table 4 and 5.

Table 4: Monthly and Annual Non-Exceedance Distributions

1-hour Mean Wind Speed

	1%	10%	20%	30%	40%	50%	60%	70%	80%	90%	91%	92%	93%	94%	95%	96%	97%	98%	99%	n(data)
Jan	1.9	4.8	6.4	7.7	9.1	10.5	11.8	13.1	14.5	16.6	16.8	17.2	17.6	17.9	18.2	18.7	19.3	20.0	21.3	46872
Feb	1.7	4.2	5.9	7.3	8.6	9.7	11.0	12.3	14.0	16.2	16.5	16.7	17.1	17.6	17.9	18.4	19.1	20.0	21.4	42659
Mar	1.5	3.7	5.2	6.5	7.6	8.8	10.0	11.3	12.9	15.1	15.6	15.9	16.3	16.7	17.4	17.9	18.7	19.6	21.1	46872
Apr	1.4	3.3	4.6	5.6	6.6	7.6	8.7	10.0	11.4	13.7	14.1	14.4	14.8	15.1	15.7	16.3	17.1	18.1	19.6	45360
May	1.2	2.9	3.9	4.9	5.7	6.6	7.6	8.8	10.2	12.3	12.6	12.9	13.3	13.7	14.2	14.6	15.4	16.2	17.7	46872
Jun	1.1	2.5	3.4	4.2	5.1	5.9	6.8	7.9	9.4	11.6	11.8	12.2	12.6	12.9	13.6	14.2	14.7	15.7	17.4	45360
Jul	1.1	2.5	3.5	4.4	5.2	6.0	6.9	8.0	9.4	11.4	11.8	12.1	12.3	12.8	13.3	13.9	14.5	15.6	17.2	46872
Aug	1.1	2.4	3.4	4.2	5.1	5.7	6.6	7.7	9.3	11.4	12.0	12.2	12.6	13.1	13.7	14.4	15.4	16.6	18.7	46872
Sep	1.1	2.6	3.7	4.6	5.4	6.4	7.4	8.6	10.0	12.2	12.5	12.8	13.3	13.9	14.4	15.1	16.0	17.3	19.6	45360
Oct	1.4	3.4	4.8	5.7	6.7	7.6	8.7	9.9	11.3	13.6	13.9	14.2	14.4	14.8	15.4	15.7	16.5	17.6	19.6	46872
Nov	1.3	3.5	4.9	5.9	7.1	8.0	9.3	10.5	12.0	14.2	14.4	14.8	15.1	15.5	16.0	16.5	17.1	18.1	19.4	45360
Dec	1.7	4.0	5.4	6.8	8.0	9.3	10.6	12.0	13.6	15.2	15.9	16.2	16.6	16.8	17.4	17.9	18.5	19.3	20.2	46848
All	1.2	3.1	4.3	5.4	6.5	7.5	8.8	10.2	11.8	14.2	14.4	14.8	15.4	15.7	16.2	16.7	17.6	18.4	20.0	552179

Table 5: Monthly and Annual Non-Exceedance Distributions

Significant Wave Height

	1%	10%	20%	30%	40%	50%	60%	70%	80%	90%	91%	92%	93%	94%	95%	96%	97%	98%	99%	n(data)
Jan	0.44	0.69	0.88	1.06	1.23	1.39	1.60	1.80	2.06	2.48	2.54	2.61	2.69	2.77	2.88	3.00	3.17	3.40	3.86	46872
Feb	0.47	0.71	0.89	1.05	1.21	1.37	1.56	1.79	2.09	2.57	2.64	2.74	2.83	2.93	3.06	3.22	3.41	3.67	4.02	42659
Mar	0.53	0.80	0.97	1.12	1.28	1.46	1.64	1.86	2.15	2.63	2.71	2.79	2.90	3.00	3.14	3.29	3.49	3.77	4.20	46872
Apr	0.61	0.91	1.07	1.19	1.32	1.46	1.60	1.77	2.03	2.42	2.48	2.56	2.65	2.76	2.88	3.02	3.20	3.47	3.94	45360
May	0.68	0.93	1.06	1.15	1.25	1.35	1.48	1.64	1.85	2.19	2.24	2.30	2.37	2.46	2.56	2.70	2.84	3.10	3.50	46872
Jun	0.81	1.00	1.11	1.18	1.27	1.36	1.47	1.60	1.78	2.16	2.21	2.28	2.34	2.42	2.51	2.61	2.77	3.06	3.57	45360
Jul	0.78	0.99	1.10	1.19	1.28	1.36	1.48	1.62	1.81	2.17	2.22	2.29	2.37	2.47	2.59	2.76	2.97	3.35	4.21	46872
Aug	0.77	1.04	1.16	1.25	1.33	1.41	1.54	1.72	2.03	2.58	2.68	2.78	2.90	3.05	3.29	3.59	3.98	4.61	5.67	46872
Sep	0.79	1.03	1.16	1.25	1.34	1.45	1.56	1.72	1.98	2.49	2.59	2.74	2.89	3.06	3.31	3.64	4.06	4.71	5.90	45360
Oct	0.74	1.02	1.17	1.28	1.39	1.51	1.65	1.82	2.06	2.55	2.63	2.71	2.79	2.86	3.01	3.21	3.44	3.76	4.41	46872
Nov	0.55	0.83	0.98	1.12	1.25	1.40	1.57	1.75	1.99	2.39	2.44	2.50	2.58	2.67	2.78	2.92	3.12	3.38	3.84	45360
Dec	0.49	0.73	0.98	1.03	1.19	1.35	1.53	1.72	1.98	2.37	2.43	2.50	2.58	2.68	2.78	2.90	3.04	3.24	3.61	46848
All	0.54	0.88	1.05	1.17	1.28	1.40	1.55	1.73	1.98	2.42	2.49	2.56	2.65	2.77	2.89	3.05	3.28	3.61	4.20	552179

(3) Summary

a. The wind in the Daini-Atsumi Knoll area comes mostly from east-southeast to southeast in the spring-autumn season, and from the west-northwest in winter.

b. The wind speed tends to be higher in the autumn-winter season than in the summer season.

c. The wave direction in the Daini-Atsumi Knoll area is mostly from east-southeast to southeasterly in the spring-autumn season, and from west-northwest more in winter.

d. The significant wave height tends to be lower in winter than in the summer and autumn season because the influence of typhoons is greater than that of monsoons.

e. The high waves and strong winds in the Daini-Atsumi Knoll are due to the effects of the typhoon.

f. The value associated with return period of 100-year for 1-hour mean wind speed is 37.3m/sec, and for significant wave height is 15.76m in the Daini-Atsumi Knoll.

g. The 99% non-exceedance distribution of the 1-hour mean wind speed is 20.0m/sec, and the 99% non-exceedance distribution of the significant wave height is 4.20m.

h. The value associated with the return period, the non-exceedance distributions, and statistical data of winds and waves were used for setting of the optimum period of offshore production tests, study for the limit condition of offshore operations, and DPS (Dynamic Positioning System) operation of the drill ship.

i. These data need to be reviewed every few years and particularly when there is a major disturbance, which would occur once ten years or one hundred years.

V.7.2 Submarine Ground

V.7.2.1 Bathymetric and Geological Survey

(1) Objective and Background

The Daini-Atsumi Knoll area is north of the eastern Nankai Trough, and we found that many lineaments and faults existed there, forming a complex seabed terrain based on the existing data including seismic survey results. Although it is known that there are submarine landslide configuration and foot print of drilling wells, detailed bathymetry and seabed features and sub-bottom geology of the these area were not sufficiently understood.

To solve these things, the bathymetric geological surveys were carried out to clarify the detail bathymetry and the seabed features for selection of the offshore production test site and study of the subsea equipment.

The survey was conducted using the “Urashima” AUV (Autonomous Underwater Vehicle) of JAMSTEC in February 2011.

However, it was presumed changes in bathymetry and subsurface sediments after the AUV survey, due to the 2011 off the Pacific coast of Tohoku Earthquake and the first offshore production test conducted.

Therefore, the new supplement detailed bathymetric geological survey was carried out in June-July 2015 using the AUV "deep 1" of Fukada Salvage Construction Co., Ltd.

(2) Details and Results

a. Details

The survey area is a 6km square including a 2km square area centered on the production test site, with an additional 3km x 4km adjacent area on the southwest side (Fig.1).

The survey was conducted using an AUV equipped with MBES (Multi Beam Echo Sounder), SSS (Side Scan Sonar), and SBP (Sub-Bottom Profiler).

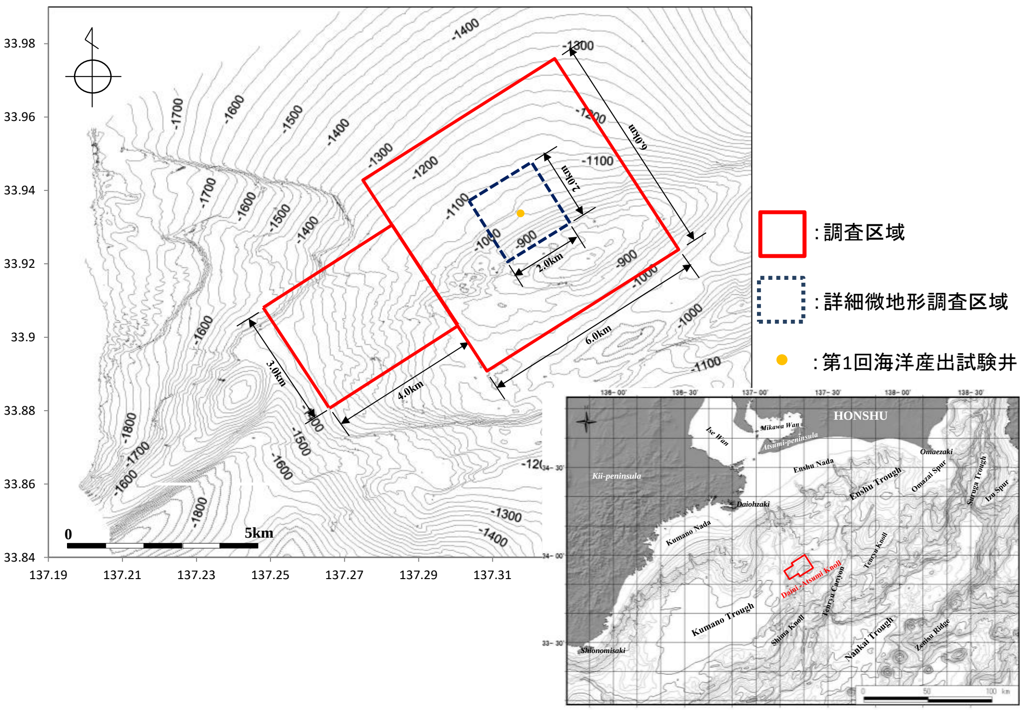

Fig.1: Survey Area

b. Results (Fig.2)

The east part of the northern slope of the knoll (a) has the offshore production test site at its west end, and based on the results of the 3D seismic surveys, its surface sediments are presumed to be a submarine landslide moving body that is not active due to blocking.

In the eastern front of the east part of the northern slope of the knoll (b), the slump layer is distributed under the seabed, and there are NNW-SSE faults and mounds.

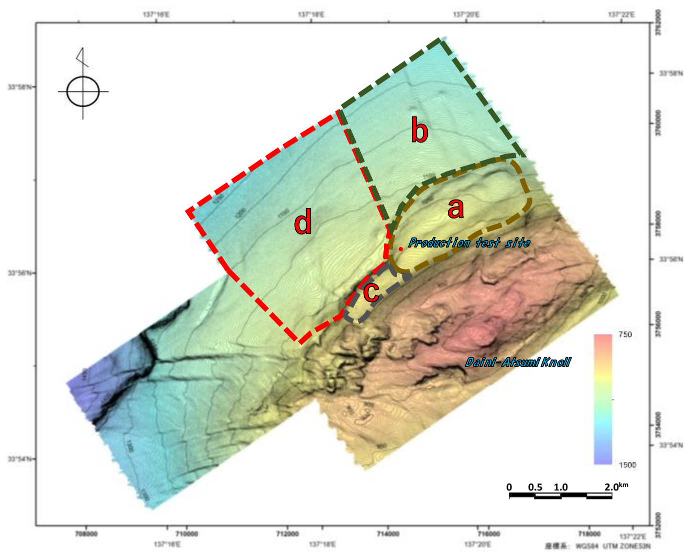

Fig.2: Bathymetric Chart

The western part of the northern slope of the knoll (c) is on the west side of the submarine landslide body, and there is a cliff at the northern part, and a talus accumulation is distributed under the cliff.

The western front of the western part of the northern slope of the knoll (d) has a thick distribution of chaotic slump layers under the seabed, and there are grabens and lineaments at the sea floor.

On the sea floor near the offshore production test site, the foot print of wells drilled in the past and the OBC (Ocean Bottom Cable) installation trace carried out at the first production test were clearly recognized.

From these survey results, it has become clear that the subsurface sediments are characterized as a mixture of carbonate crust and carbonate rocks.
As a result of the above, it is considered that the first and second production test sites are near the west end of the submarine landslide block in the area (a), and the displacement is small and the stable state is maintained.

(3) Summary
a. The production test site is located on the northern slope of the Daini-Atsumi Knoll, forming complex terrain due to uplift, faults, folds, and submarine landslides with the tectonic movement. A few grabens and many lineaments exist on the seafloor.
b. On the northern slope of the knoll, large scale slump layers formed by the submarine landslide are widely distributed under the seabed, exhibiting a chaotic structure.
c. The survey results, together with the results of the seabed boring survey and soil tests, can be used as basic data for examining the stability of the seabed floor, and should be very useful for improving the accuracy of the geohazard assessment.

References
[1] E. Shimura, K. Suzuki (2015) : The characreristic of bottom topography and sediments on the northwester slope of Daini-Atsumi Knoll, and case study of seabed ground stability, The 7th Comprehensive Symposium on Methane Hydrate (CSMH-7), AIST, pp.121-125.
[2] E. Shimura, K. Suzuki (2016): The features of submarine landslide on the northwest slope of Daini-Atsumi Knoll, and its cover sediments, Japan Geoscience Union Meeting 2016.

V.7.2.2 Seabed Boring Survey and Geomechanical Tests
(1) Objective and Background
MH Offshore production tests are conducted at relatively shallow depths below the seabed. As a result, deformation of the seabed floor is expected. Therefore, the stability of the seabed floor is one of the critical conditions required at the test site. Therefore, mechanical behavior and response of the geological formations around wells are important research subjects.
The following technical problems exist due to large pressure reduction for the formation several hundred meters below the seabed.
a. Well stability assessment: Can the formation from the seabed to the MH layer support the well's weight?
b. Characteristics of the sealing layer: Define the characteristics of the sealing layer to apply the decompression method
c. Stratum deformation due to decomposition of MH: Study of the impact of reservoir consolidation due to decomposition of MH in shallow layers

d. Slope stability assessment: Acquire basic data of submarine landslide risk and geo-hazard assessment.
In order to study these technical issues, it was decided to recover soil samples and carry out an in-situ cone penetration test from the surface to the top of the MH layer at the production test site. And those samples, as well as some samples taken in previously drilled holes, were used to perform geo-mechanical tests.

(2) Details and Results

a. Details

1) The survey points were as follows:
six points around the offshore production test site: AT-GT1, AT1-GT1A, AT1-GT2, AT1-GT2A, AT1-GT2B, AT1-GT3.

2) Two points around the trace of the large-scale submarine landslide area (approximately 6km west from test site): TS-GT1, ATS-GT1A.

3) Core samples were recovered at these points, and in some wells, in-situ cone penetration tests *1 (CPT: Cone Penetration Test) were conducted using Dolphin System^{TM} (Fig. 1) by FUGRO-McCLELLAND. MARINE GEOSCIENCES INC.)

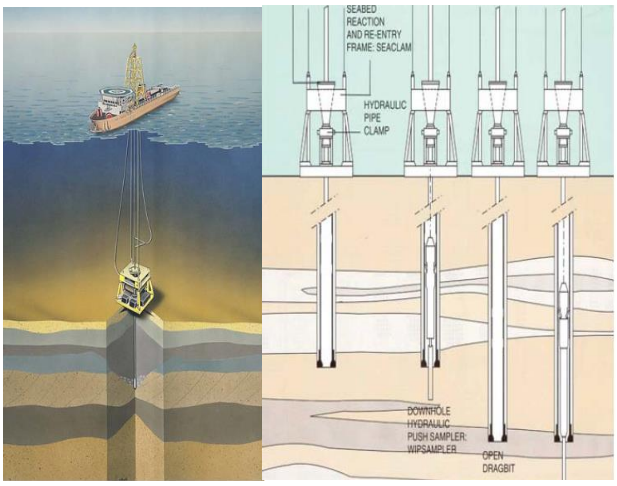

Fig.1　Dolphin system^{TM}（Fugro）

*1: CPT is one of the in-situ tests. It directly pierces the seabed floor using an electric static cone and measures three components [penetration resistance (qt), frictional resistance (fs), pore pressure (u)].

b. Results

The results obtained from the tests are as follows:

1) The marine clay contained in those core samples in the Daini-Atsumi Knoll area are significantly different in terms of properties from other marine clays, and this suggests that the seabed floor of this area is rich in diatom fossils, calcareous nannofossils, and carbonate sediments.

2) The core samples of this area have a low plasticity index and activity.

3) The over consolidation ratio (OCR) is measured and it was found that the OCR in this area is generally high, especially at shallow depths.

4) The maximum stress ratio decreases with depth.

5) The maximum stress ratio at failure decreases as the sampling depth increases.

6) The undrained shear strength in this area increases with depth, however the rate of strength increase tends to be asymptotically to a value around 0.6-0.7 with depth increase. However, this result is a significantly larger value than that for marine clay off the coast of Japan.

(3) Summary

a. The core samples were subjected to various physical and geo-mechanical tests, core analysis, etc. at AIST, Institute of Technology of Shimizu Construction co. Ltd., Universities of Kyoto, Yamaguchi, and Hokkaido.

b. These results were comprehensively interpreted together with results of the 3D seismic survey and the detailed bathymetric/geological survey at the Daini-Atsumi Knoll.

c. As a result, the offshore production test site is considered to be located on the blocked mass movement of submarine landslide on the slope of northern part of the Daini-Atsumi Knoll.

d. On the other hand, on the northwest slope of the Daini-Atsumi Knoll, slump layers originating from the submarine landslide are widely deposited under the seafloor, and they show a characteristic with exhibiting a chaotic sedimentary structure, and for this reason the upper layer are largely deformed.

e. Many grabens and lineaments were recognized in the seafloor where the slump layer is distributed.

f. The results of these studies and analyses are reflected in the offshore production test plan, drilling plan, well design, and other documents.

References

[1] Long, X., Tjok, K.-M., Trandafir, A.C., Sato, R. & Yamamoto, K. 2014. Evaluation of Geological and Geotechnical Characteristics for Deepwater Sediments in Offshore Japan, *The 24th International Ocean and Polar Engineering Conference*, Busan, Korea, June 15 - June 20, 2014.

[2] Shimizu Construction Co., Ltd. (2011): The report of geo-mechanical tests for the first offshore seafloor production test.

[3] Department of Civil Engineering of College of Industrial Technology, Nihon University (2011): The report of planning and analysis for geo-mechanical tests on seabed boring core samples.

[4] OYO Co., Ltd. (2011): The report of geo-mechanical tests for core samples collected in the seabed boring survey.

[5] Prof. Hiroyuki Tanaka, Environmental Field Engineering Division, Graduate School of Engineering, Hokkaido University (2011): The report of the results for constant strain rate consolidation test conducted for the planning of the fro-mechanical test on the seabed boring core samples.

[6] Prof. Masayuki Hyodo, Environment Symbiosis, Graduate School of Technology for Engineering, Yamaguchi University (2012): The report of the results for consolidation and non-drainage triaxial compression test conducted for planning of the geo-mechanical tests on seabed boring core samples.